VOL 5, NO.1 (March 2025) 1-33
https://jagst.utm.my

JAGST
Journal of Advanced Geospatial Science & Technology

Geospatial Analysis of NDVI-Rainfall Dynamics under High ENSO Influence in Peninsular Malaysia

Zulfaqar Sa'adi[1*], Nor Eliza Alias[1,2], Zulkifli Yusop[1,2], Lelavathy Samikan Mazilamani[2], Mohamad Rajab Houmsi[3,4], Lama Nasrallah Houmsi[5], Shamsuddin Shahid[2], Azmi Aris[1,2], Muhammad Wafiy Adli Ramli[6], Najeebullah Khan[7], Prabhakar Shukla[8], Zainura Zainon Noor[1,9*]

[1]Centre for Environmental Sustainability and Water Security, Research Institute for Sustainable Environment, Universiti Teknologi Malaysia, 81310 Johor Bahru, Johor, Malaysia
[2]Department of Water and Environmental Engineering, Faculty of Civil Engineering, Universiti Teknologi Malaysia, 81310 Johor Bahru, Johor, Malaysia
[3]Center for River and Coastal Engineering (CRCE), Universiti Teknologi Malaysia, 81310 Johor Bahru, Johor, Malaysia
[4]New Era and Development in Civil Engineering Research Group, Scientific Research Center, Al-Ayen University, Thi-Qar, Nasiriyah, 64001, Iraq
[5]Finance and Banking Department, College of Economics, Aleppo University, Aleppo Halab Syria, Mouhafaza, 15310, Syrian Arab Republic
[6]Geography Section, School of Humanities, Universiti Sains Malaysia, 11700, Penang, Malaysia
[7]Faculty of Civil Engineering, Universiti Teknologi Malaysia, 81310 Johor Bahru, Johor, Malaysia
[8]Department of Civil Engineering, Indian Institute of Technology (IIT) Delhi, Hauz Khas, Delhi 110016, India
[9]Faculty of Chemical and Energy Engineering, Universiti Teknologi Malaysia, 81310 Johor Bahru, Johor, Malaysia

*Corresponding author: zainurazn@utm.my; zulfaqar@utm.my

Abstract **–** Peninsular Malaysia (PM) rainfall varies significantly due to El Niño-Southern Oscillation (ENSO), making it an important region to study the relationship between Normalized Difference Vegetation Index (NDVI) and rainfall. These connections are complex, spatially non-linear, non-stationary, and scale-dependent, challenging conventional regression models. A local modelling approach, Geographically Weighted Regression (GWR), was employed to address this, accommodating spatial relationship variability. This study utilizes the CMORPH gridded dataset to explore the NDVI-rainfall relationship in PM during very strong El Niño events of 2015/2016 and strong La Niña events of 2010/2011. During the El Niño 2015/2016 event, the Gaussian weighting function achieved an Akaike Information Criterion (AIC) of 398.48 and a quasi-global R^2 of 0.63, outperforming the Bisquare function's AIC of 434.12 and quasi-global R^2 of 0.48. In the La Niña 2010/2011 event, the Bisquare function excelled with an AIC of 442.01 and a quasi-global R^2 of 0.52, while the Gaussian recorded an AIC of 505.69 and a quasi-global R^2 of 0.10. The median local Coefficient of Determination (local R^2) for El Niño (0.6 to 0.8) was higher than that for La Niña (some areas dropping below 0.4), highlighting the GWR model's superior performance in capturing spatial variation. In terms of predictive power, the metrics demonstrate superior model performance during El Niño, with a Mean Absolute Error (MAE) of 0.5, a Root Mean Square Error (RMSE) of 0.66, Coefficient of Determination (R^2) value of 0.63 indicating significant variance explained, and Nash-Sutcliffe Efficiency (NSE) and the Kling-Gupta Efficiency (KGE) both equal to 0.63 and 0.6, respectively.

Keywords *– CMORPH, ENSO, Geographically Weighted Regression, NDVI, Peninsular Malaysia, Rainfall*

Article History: Received 7 November 2024, Accepted 26 December 2024, Published 28 March 2025

How to cite: Sa'adi, Z., Alias, N. E., Yusop, Z., Mazilamani, L. S., Houmsi, M. R., Houmsi, L. N., Shahid, S., Aris, A., Ramli, M. W. A., Khan, N., Shukla, P. and Noor, Z. Z. (2025). Geospatial Analysis of NDVI-Rainfall Dynamics under High ENSO Influence in Peninsular Malaysia. Journal of Advanced Geospatial Science & Technology. 5(1), 1-33.

1.0 Introduction

Adequate rainfall supports plant life and increases vegetation cover (Muhammad et al., 2020). On the other hand, insufficient or irregular rain can lead to drought conditions, negatively affecting vegetation (Bechtold, 2018). However, the high spatial variability in the rainfall distribution across an area can influence the types of vegetation that thrive in tropical regions (Gaviria et al., 2017). This intricate relationship underscores the significance of understanding how rainfall patterns affect the vitality and composition of vegetation, contributing to a broader comprehension of ecosystem dynamics. To assess the influence of rainfall variations on vegetation growth, it is imperative to conduct an analysis examining the spatial correlation between vegetation and rainfall (Muhammad et al., 2020). The quantification of vegetation levels can be derived using vegetation indices such as the Normalized Difference Vegetation Index (NDVI) (Pang et al., 2017). The NDVI is a widely utilized proxy for vegetation greenness across diverse regional and global studies. Numerous studies have used time series NDVI derived from various satellite sources as dependent variables in investigations exploring the relationship between NDVI and rainfall (Mallick et al., 2021; Georganos et al., 2017; Zhang et al., 2017; Moses et al., 2022). Most works discovered a robust and more predictable relationship between rainfall and NDVI when an appropriate spatial scale is employed. Consequently, multi-spectral satellite data with medium spatial resolution, such as Moderate Resolution Imaging Spectroradiometer (MODIS) imagery, can be considered more suitable for obtaining improved NDVI values (Lamchin et al., 2015).

The variation in NDVI is impacted by prevailing climatic conditions such as rainfall and temperature, and this correlation is consistently observed across various spatial and temporal scales (Gaviria et al., 2017). Rainfall is crucial in predicting vegetation distribution, particularly in Peninsular Malaysia (PM) (Lion et al., 2017). Given the region's tropical climate, characterized by distinct wet and relatively dry monsoons which can be exaggerated by the large-scale climate phenomena like the El Niño-Southern Oscillation (ENSO) events, the amount and distribution of rainfall directly impact the health and composition of vegetation (Arjasakusuma et al., 2018). In this context, the severe weather occurrences linked to ENSO, such as droughts triggered by El Niño or heavy rainfall caused by La Niña, contribute to fluctuations in vegetation health and composition (Boyd et al., 2002). Indeed, it has been observed that the variations in rainfall patterns influence soil moisture levels, which, in turn, affect plant growth and ecosystem dynamics (Wang and Hamzah, 2018; Marryanna et al., 2019). The interplay between rainfall and vegetation is intricate,

as different plant species exhibit varying responses to the duration and intensity of rainfall. Therefore, the inclusion of ENSO events needs to be investigated to further understand its impact on the NDVI-rainfall relationship.

While numerous studies describe the connection between NDVI and rainfall, they frequently utilize worldwide linear models adjusted through ordinary least squares (OLS) regression techniques (Mallick et al., 2021; Udelhoven et al., 2009; Balaghi et al., 2008). Yet, the spatial and temporal fluctuations in the relationship between NDVI and rainfall depend on additional factors such as vegetation composition, land cover, soil type, terrain characteristics, human influence, and microclimatic conditions. Models assuming stationarity may inadequately capture the true nature of these relationships, raising concerns about the validity of their results. The sensitivity of environmental change in PM to fluctuations in rainfall, particularly under the influence of ENSO phenomena like El Niño and La Niña, is a critical aspect of ecological dynamics in the region. The tropical climate of PM, characterized by distinct wet and dry seasons, makes rainfall a key determinant of environmental health (Mohd Razali et al., 2016). The influence of ENSO events, such as El Niño-induced droughts or La Niña-driven heavy rainfall, adds a layer of complexity to this relationship. Compared to other regions, the greening of the tropics due to increased rainfall is not well studied in PM. It is assumed that heightened rainfall levels may contribute to the proliferation of herbaceous and tree cover (Chew et al., 2022; Wang and Hamzah, 2018). The increase in rainfall is a primary mechanism driving this observed greening, creating a conducive environment for vegetation growth. Infusing moisture into the soil enhances soil fertility and provides the conditions for plant germination, growth, and reproduction (Born et al., 2015; Marryanna et al., 2019).

The intricate and spatially diverse connection between NDVI and rainfall has not been extensively explored in tropical regions, particularly in PM. To address this gap, this study employs GWR, a local non-parametric regression method that facilitates a detailed analysis of these relationships (Georganos et al., 2017; Zhao et al., 2015). Widely used in human geography and gaining popularity in ecology, GWR accommodates spatial variability, offering a better understanding of non-stationary relationships. The study focuses on the PM from 2000 to 2022, emphasizing the impact of ENSO events, specifically the El Niño and La Niña events. These extreme periods were chosen to capture substantial differences in total rainfall during contrasting ENSO events, facilitating the examination of temporal changes in spatial correlations. The study

compares Gaussian and Bisquare weighting within the GWR framework to evaluate which scheme more effectively captures the spatial relationships between NDVI and rainfall under varying climatic conditions. By mapping local regression outcomes, the research seeks to pinpoint regions within PM that display specific sensitivity to changes in rainfall, providing valuable understanding into the NDVI-rainfall dynamics under extreme influence of ENSO.

2.0 Study Area

The research focuses on PM, with its district boundaries shown in Figure 1. PM is situated in Southeast Asia and covers the southern part of the Malay Peninsula (Houmsi et al., 2023). The South China Sea borders the east coast of PM. PM covers an approximate area of 131,598 km2 and comprises eleven states and two federal territories. The region's topography ranges from coastal plains and lowlands to hilly and mountainous terrain. Notable mountain ranges include the Titiwangsa and the Banjaran Bintang Range in the north. This region experiences a tropical climate influenced by the Northeast Monsoon (NEM) and Southwest Monsoon (SWM) seasons (Muhammad et al., 2022). The NEM commonly takes place between November and March, resulting in substantial rainfall in the states along the east coast, including Kelantan, Terengganu, Pahang, and the eastern region of Johor. The SWM brings rainfall to the west coast states such as Penang and Selangor. Exploring the NDVI-rainfall relationship in PM during the NEM is crucial for understanding this region's unique climatic patterns and ecological implications.

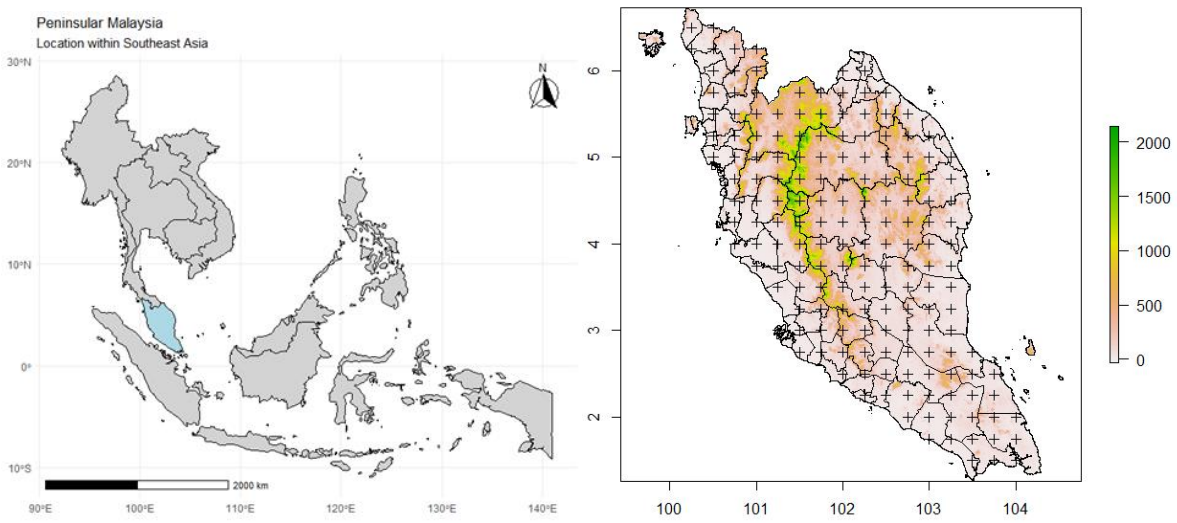

Figure 1. The PM is located within Southeast Asia with 170 grid points of gridded-based satellite CMORPH rainfall dataset, district boundary, and elevation based on Shuttle Radar Topography Mission (SRTM) at 90 m spatial resolution.

3.0 Data and Sources

3.1 Gridded-Based Satellite CMORPH Rainfall Data

Of the available remote sensing precipitation datasets, CMORPH data stands out with its sufficient spatial resolution and extensive coverage, making it a preferred choice among researchers (Gumindoga et al., 2019a; Gumindoga et al., 2019b; Pereira Filho et al., 2018). The Climate Data Record (CDR) for Satellite Precipitation - CMORPH comprises satellite-derived precipitation estimates that have undergone bias correction and reprocessing through the Climate Prediction Center (CPC) Morphing Technique (MORPH). This process results in a global, high-resolution precipitation analysis (Source: https://www.ncei.noaa.gov/access/metadata/landing-page/bin/iso?id=gov.noaa.ncdc:C00948) (Joyce et al., 2004). The data is reprocessed on a global grid with a spatial resolution of 8×8 km (0.25°), and the daily data was utilized for the current study with 170 grid points located within the PM was downloaded, extracted, and then summed into monthly value for the duration of selected ENSO event (section 3.3).

3.2 Normalized Difference Vegetation Index (NDVI)

In PM, rainfall is the primary source of soil and surface water. The presence of water significantly influences vegetation growth. Typically, higher rainfall results in increased soil moisture, leading to more robust plant growth. Conversely, reduced rainfall tends to hamper vegetation growth. Consequently, changes in rainfall serve as a crucial indicator of vegetation growth conditions (Wang and Hamzah, 2018). The normalized vegetation index is a metric that assesses vegetation by quantifying the variance between the near-infrared and red bands, indicating regional vegetation growth. This research used the normalized vegetation index to depict vegetation growth (Huang et al., 2021). Within this context, NIR represents the reflectivity of the near-infrared band, and Red corresponds to the reflectivity of the red band. The NDVI value ranges from -1 (indicating water bodies) to 1 (suggesting dense vegetation). The NDVI data employed in this investigation is obtained from atmospherically corrected reflectance in the red and near-infrared wavebands captured by the MODIS sensor on board the Terra satellite (Lamchin et al., 2015). In this study, the

Vegetation Indices Monthly L3 Global 1km (MOD13A3), a monthly NDVI product at 1 km spatial resolution, was extracted for the selected ENSO events (section 3.3), which was obtained from http://modis-land.gsfc.nasa.gov/vi.html. The NDVI value was spatially extracted to match the 170 grid points of CMORPH data. The NDVI was integrated with the duration of the respective ENSO events to measure vegetation productivity for each selected event.

3.3 El Niño and La Niña Years

The PM climate is significantly influenced by the ENSO, with El Niño (La Niña) periods often producing drier and warmer (or wetter and cooler) temperatures (Tan et al., 2021). In this study, very strong 2015/2016 (June 2015 to May 2016), along with the strong La Niña events of 2010/2011 (June 2010 and June 2011), respectively, were evaluated to assess the NDVI-rainfall relationship (Khor et al., 2021).

4.0 Methods

4.1 Procedure

The following procedure outlines the methodological framework adopted to analyze the relationship between rainfall and NDVI dynamics under the influence of ENSO events in PM. The research flowchart is presented in Figure 2. This study integrates gridded rainfall (CMORPH) and NDVI (MOD13A3) datasets, spatial statistical analyses, and GWR to examine the spatial variability, autocorrelation, and localized relationships during the El Niño (2015/2016) and La Niña (2010/2011) phases. The step-by-step approach includes data preprocessing, model development, performance evaluation, and visualization to understand NDVI-rainfall interactions under extreme climate conditions comprehensively. The procedure is as follows:

1. Gridded rainfall data from CMORPH and NDVI data from MOD13A3 were collected. Both datasets were gridded to a spatial resolution of 0.25 degrees using bilinear interpolation for spatial consistency.
2. Spatial descriptive statistical analysis was conducted to evaluate the spatial variability of rainfall and NDVI, including the computation of mean, median, standard deviation (SD), skewness, and coefficient of variation (CV). Moran's I and Geary's C indices also assessed spatial autocorrelation patterns in the rainfall and NDVI datasets.

3. The GWR model was developed using an adaptive kernel to analyze the relationship between rainfall and NDVI. Two weighting functions, Gaussian and Bisquare, were tested to identify the optimal model performance. Model evaluation and comparison were conducted using selection criteria such as Akaike Information Criterion (AIC), Corrected Akaike Information Criterion (AICc), Quasi-global R^2, Residual Sum of Squares (RSS), Effective Number of Parameters (traceS), and Sigma (model: traceS).
4. Using the optimized GWR model, two ENSO events, El Niño (2015/2016) and La Niña (2010/2011), were selected to examine the dynamics of NDVI-rainfall relationships under contrasting ENSO phases. The GWR results for each event were compared with OLS regression models, and the comparison was statistically evaluated using the analysis of variance (ANOVA) test to identify significant differences between the models.
5. The performance of the GWR model was assessed using local Coefficient of Determination (local R^2) values and rainfall coefficients. Predicted NDVI values (iNDVI) were validated against performance metrics, including Mean Absolute Error (MAE), Root Mean Square Error (RMSE), Coefficient of Determination (R^2), Nash-Sutcliffe Efficiency (NSE), and Kling-Gupta Efficiency (KGE). An ENSO and iNDVI map were also created to visualize spatial patterns under the influence of the El Niño and La Niña events.

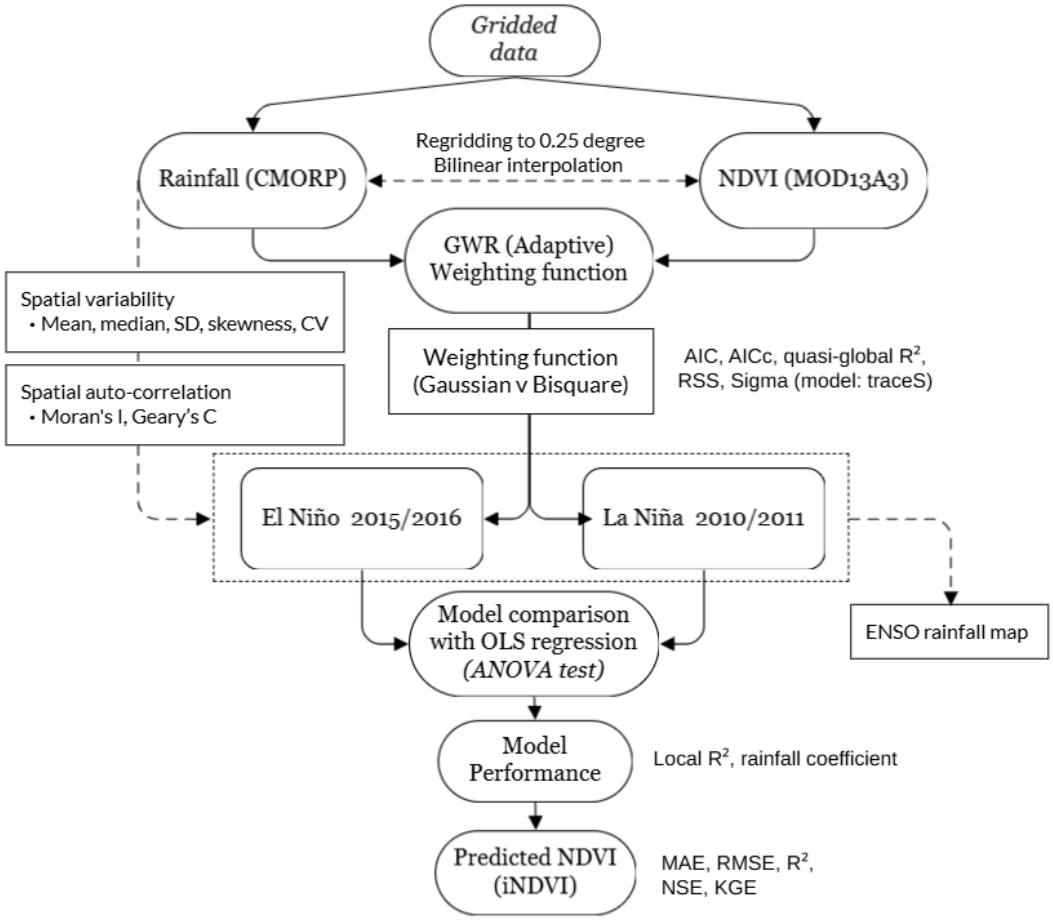

Figure 2. Research flowchart.

4.2 Test of Spatial Autocorrelation

Moran's I statistic is employed as a spatial autocorrelation measure to assess the spatial dispersion of rainfall during each ENSO event (Soibam et al., 2015). This statistic evaluates the degree of similarity between the rainfall values at different grid points to describe the spatial patterns of dispersion, whether they exhibit clustering, randomness, or dispersion. Moran's I range from -1 (indicating perfect dispersion) to 1 (indicating ideal clustering), with 0 representing a spatially random pattern. The analysis involves calculating observed Moran's I values, expected values under spatial randomness, standard deviation, and p-values to determine the statistical significance of the observed spatial autocorrelation of the NDVI-rainfall relationship. This spatial assessment aids in characterizing the spatial relationships and patterns of rainfall across the study area during the selected ENSO events. The formula for Moran's spatial autocorrelation coefficient, denoted as *I*, is as follows:

$$I = \frac{\sum_{i=n}^{j} n(R_i - \bar{R})(R_j - \bar{R})}{\sum_{i=n}^{n} J(R_i - \bar{R})^2} \quad (1)$$

In this formula, n represents the total number of areas, J is the total number of joints, R_i and R_j are the rainfall depths in two adjacent areas, and $\overline{R}$ denotes the overall mean of rainfall.

In addition to Moran's I, Geary's C (Yamada, 2024) was employed to assess spatial autocorrelation, measuring the degree of spatial dependency or clustering in geospatial data. It is particularly effective for identifying how similar or dissimilar values are positioned near each other across a spatial landscape, making it suitable for examining the spatial patterns of NDVI and rainfall dynamics under high ENSO influence. This study will calculate Geary's C to assess the spatial autocorrelation of NDVI and rainfall values and understand how neighbouring data values exhibit similarity or dissimilarity. The formula for Geary's C is given as:

$$c = \frac{(n-1)}{2\sum_i \sum_j w_{ij}} \frac{\sum_i \sum_j w_{ij}(x_i - x_j)^2}{\sum_i (x_i - \bar{x})^2} \quad (2)$$

Where n represents the total number of spatial units, w_{ij} denotes the spatial weights between locations i and j, x_i and x_j are the values of the variable (either NDVI or rainfall) at each location, and $\bar{x}$ is the variable's mean. Geary's C values range from 0 to 2, with a value of 1 indicating no spatial autocorrelation, values below 1 suggesting positive spatial autocorrelation (similar values cluster together), and values above 1 pointing to negative spatial autocorrelation (dissimilar values are more likely to be neighbours). This measure provides clarity into the spatial clustering or dispersion of NDVI and rainfall anomalies during ENSO phases, helping to identify regions where spatial patterns may strongly influence vegetation responses to rainfall variations. The local sensitivity of Geary's C makes it an ideal complement to global measures like Moran's I, allowing for a more detailed understanding of spatial variations in NDVI-rainfall relationships under extreme climate conditions in PM (Bhatti et al., 2024).

4.3 Weighting Method

This study compared Gaussian and Bisquare weighting functions in GWR to model the relationship between NDVI and rainfall across different spatial locations across PM. These functions help determine the influence of neighbouring data points based on their distance, allowing for a more detailed understanding of spatial variability. The Gaussian weighting method in GWR assigns

weights to data points based on a Gaussian, or Normal, distribution, where the influence of each point decreases smoothly and continuously with increasing distance from the focal point (Mondiana et al., 2024). One of the key advantages of the Gaussian weighting method is its smooth weight decay, which provides a gradual and continuous decrease in influence as distance increases (Geniaux, 2024). This characteristic makes it particularly useful for capturing broader spatial trends while maintaining local detail, as it allows for a flexible adjustment of the bandwidth to control the spread of influence. The Gaussian weighting method is also well-understood due to its foundation in the widely used Gaussian distribution. It is particularly suitable for studies where a gradual change in influence with distance is expected, providing a balanced approach that effectively captures local variations and broader spatial patterns. This method is ideal for spatial analyses that require a detailed understanding of spatial heterogeneity, as it ensures a smooth transition in weights, thereby minimizing abrupt changes and potential discontinuities in the modelled relationships.

On the other hand, the Bisquare function applies weights that decrease to zero beyond a certain distance, providing compact support. It limits the influence of points beyond a specific threshold, ensuring that only nearby points significantly impact the regression results (Mondiana et al., 2024). This approach is efficient when distant data points should not influence the local regression model. By sharply reducing the influence of points further away, this method helps capture the local variations more accurately. Studies such as Xu et al. (2015) have utilized this function to exclude the influence of distant points entirely. For model comparison, the studied ENSO events were used to evaluate the performance of different weighting methods. The comparison was based on several metrics, including the AIC, AICc, Quasi-global R^2, RSS, traceS, and Sigma (model: traceS).

4.4 Geographically Weighted Regression

GWR functions as a localized spatial statistical method tailored to examine spatial non-stationarity. It extends and enriches conventional multiple linear regression analysis by directly describing and clarifying the quantitative connections among spatial variables. Additionally, GWR provides uncertainty assessments for the estimated regression coefficients while offering enhanced computational adaptability. This approach efficiently scrutinizes the geographical associations involving precipitation and key variables like latitude, longitude, and elevation above sea level.

According to Georganos et al. (2017), GWR is useful for evaluating spatial relationships in geographical datasets due to its versatility in capturing localized changes. As of now, GWR has been extensively employed to investigate spatially varying relationships between NDVI and climatic factors in diverse regions, including North China (Zhao et al., 2015), U.S. Central (Kang et al., 2014), Saudi Arabia (Mallick et al., 2021), and Africa (Georganos et al., 2017). A complete presentation of the GWR method was documented by O'Sullivan (2003). A brief explanation of GWR is offered here. A simple statistical model, referred to as a "global model", can be explained by one explanatory variable as follows:

$$y_i = a + bx_i + \varepsilon_i, \ i=1 : n \quad (2)$$

Where y represents the dependent variable, x represents the independent variable or explanatory factor, ε denotes the error term, a and b are the parameters subject to estimation, and n signifies the number of samples corresponding to spatial locations.

The above model is calibrated using OLS regression, where parameters a and b are estimated to minimize the sum of the squares of the model residuals (Georganos et al., 2017). In OLS, the estimation of these parameters is expressed through a set of matrix equations, with the calculation of parameter b as presented in Equation (3) below:

$$\hat{b} = (X^T X)^{-1} X^T Y \quad (3)$$

Here, $\hat{b}$ represents the estimated value of b; X denotes the vector containing the values of the independent variable, and Y represents the vector containing the values of the dependent variable. $\hat{b}$ stays constant throughout the research area, represents the rate at which the dependent variable changes with a one-unit variation in the independent variable. This parameter estimate particularly relates to the rainfall-NDVI relationship in the empirical example of this research.

GWR generates an individual regression equation for each observation, with each equation calibrated using a distinct weighting of the observations within the dataset. The expressions for each GWR equation may take the form:

$$y_i = a\,(u_i, v_i) + b\,(u_i, v_i) x_i + \varepsilon_i\,, \ i = 1 : n \quad (4)$$

Where the coordinates of location i are denoted by $(u_i,\ v_i)$ and the local parameters that need to be estimated, specifically for location i , are $a(u_i,\ v_i)$and $b(u_i,\ v_i)$. This is achieved by

establishing and fitting a sub-model centred on each observation site, utilizing a subset of the initial observations. The sub-model investigation region is formed by a neighbourhood defined through a weighting technique, where neighbouring observations hold a non-zero weight. Typically, the number of submodels corresponds precisely to the number of observations. Therefore, Equation (4) can be rephrased as follows:

$$\hat{b}(u_i, v_i) = (X^T W(u_i, v_i) X)^{-1} X^T W(u_i, v_i) y \quad (5)$$

In this equation, $\hat{b}$ represents a vector comprising local estimates of $b(u_i,\ v_i)$, and the data weights for the regression point *i* (sub-model *i*) are specified by the weights matrix $W(u_i,\ v_i)$. A continuous distance function dictates these weights, assigning higher weights to observations closer to the regression point *i* and lower weights to those at a greater distance.

In GWR, the selection of weighting is pivotal as it delineates the neighbourhood. Commonly used weighting functions encompass Gaussian, Gaussian-like, or bi-square options. For instance, O'Sullivan (2003) suggested the following weighting function, which is Gaussian-like:

$$w_{ij} = exp\left[-\frac{1}{2}\left(\frac{d_{ij}}{b}\right)^2\right] \quad (6)$$

Here, w_{ij} represents the weight assigned to observation *j* in relation to the sub-model for location *i*; d_{ij} indicates the Euclidean distance between *j* and *i*, and *b* represents the size of the neighborhood. However, most GWR software utilizes the bi-square function, defined as follows:

$$w_{ij} = \left[1 - \left(\frac{d_{ij}}{b}\right)^2\right] \quad \text{if } d_{ij} < b \quad (7)$$

$$= 0 \text{ elsewhere}$$

In GWR terminology, the term "kernel" is used to denote the neighbourhood, while the maximum distance from the regression location i is termed the "bandwidth" (Georganos et al., 2017). Two categories of kernels are available for use: a "fixed kernel," which delineates the neighbourhood with a circular boundary having a radius equal to the bandwidth, making it more suitable for evenly distributed spatial data like gridded data, and an "adaptive kernel," where the neighbourhood is defined by the count of nearest neighbours, making it more suitable for data with varying spatial density such as centroids of administrative boundaries. Different types of kernels use distinct weighting schemes. Continuous weighting functions allow parameter estimation at

locations beyond the observed points. The choice of bandwidth size is critical, as an excessively large bandwidth may lead to a global model with increased bias. In contrast, a bandwidth that is too small may result in less biased but more variable estimates with more significant standard errors (Georganos et al., 2017).

4.5 Model Comparison

The F-test, based on ANOVA, was conducted to evaluate and compare the relative performance of models, specifically assessing the statistical significance of any observed improvements:

$$F = \frac{\frac{RSS_{gwr}}{DF_{gwr}}}{\frac{RSS_{glm}}{DF_{glm}}} \quad (8)$$

In this context, RSS_{gwr} represents the RSS for a GWR model, RSS_{glm} signifies the RSS for a global model, while DF_{gwr} and DF_{glm} denote the degrees of freedom for the GWR and global models, respectively.

4.6 Evaluation of Predicted Pattern

To test the prediction accuracy of GWR in predicting iNDVI, three output indices, namely, MAE, RMSE, R^2, NSE, and KGE. In addition, the spatial mapping of the observed iNDVI and the predicted iNDVI was mapped for assessment.

5.0 Results and Discussion

5.1 Spatial Variability of Rainfall in PM

Spatial rainfall variability in PM reveals significant patterns characterized by positive spatial autocorrelation and clustering. The Moran's I value of 0.282 indicates a moderate level of spatial autocorrelation, suggesting that areas with similar rainfall patterns are geographically clustered rather than randomly distributed. This clustering is further supported by Geary's C statistic of 0.7107, which reflects a tendency for nearby locations to exhibit similar rainfall characteristics. Such local spatial relationships indicate that certain regions experience consistent rainfall patterns. Furthermore, the mean, median, SD, skewness, and CV were analyzed and mapped to assess spatial heterogeneity in rainfall distribution, as illustrated in Figure 3. The mapping of mean and median monthly rainfall distributions reveals apparent differences between the eastern and western sections of the study area. Mean rainfall values span from 174 to 338 mm, with specific locations exhibiting

notably higher averages. Likewise, median rainfall ranges from 162 to 273 mm, with the northern region consistently demonstrating greater median values than other areas.

The northern and northeastern regions of PM receive the highest levels of rainfall, with mean values surpassing 300 mm. As one moves southward and westward, rainfall amounts gradually decline. In contrast, the central and southern regions experience relatively lower rainfall, generally between 200 mm and 250 mm. The northern and northeastern areas also display the highest median rainfall, exceeding 260 mm, while median values decrease in the southern and western directions, typically ranging from 180 mm to 220 mm. This distribution underscores significant regional disparities in mean and median monthly rainfall, with the northern and northeastern regions receiving substantially more rainfall than other parts of the PM. The SD values vary from 67 to 273 mm, reflecting differences in rainfall variability across the landscape, with some regions experiencing more erratic patterns than others. Skewness values, ranging from 0.03 to 2.21, indicate the asymmetry of rainfall distribution; positive skewness signifies a longer tail on the right side of the distribution, indicating occasional heavy rainfall events, whereas negative skewness suggests a longer left tail, denoting more frequent lighter rain. CV values range from 0.35 to 0.96, with lower values reflecting a more uniform rainfall distribution and higher values indicating more significant variability. Overall, the spatial analysis reveals a concentration of higher mean, SD, skewness, and CV values in the northeastern region, highlighting areas more susceptible to variable and potentially intense rainfall patterns. In contrast, the northern region consistently shows higher median rainfall values, suggesting a tendency for more reliable and consistent rainfall amounts in that area.

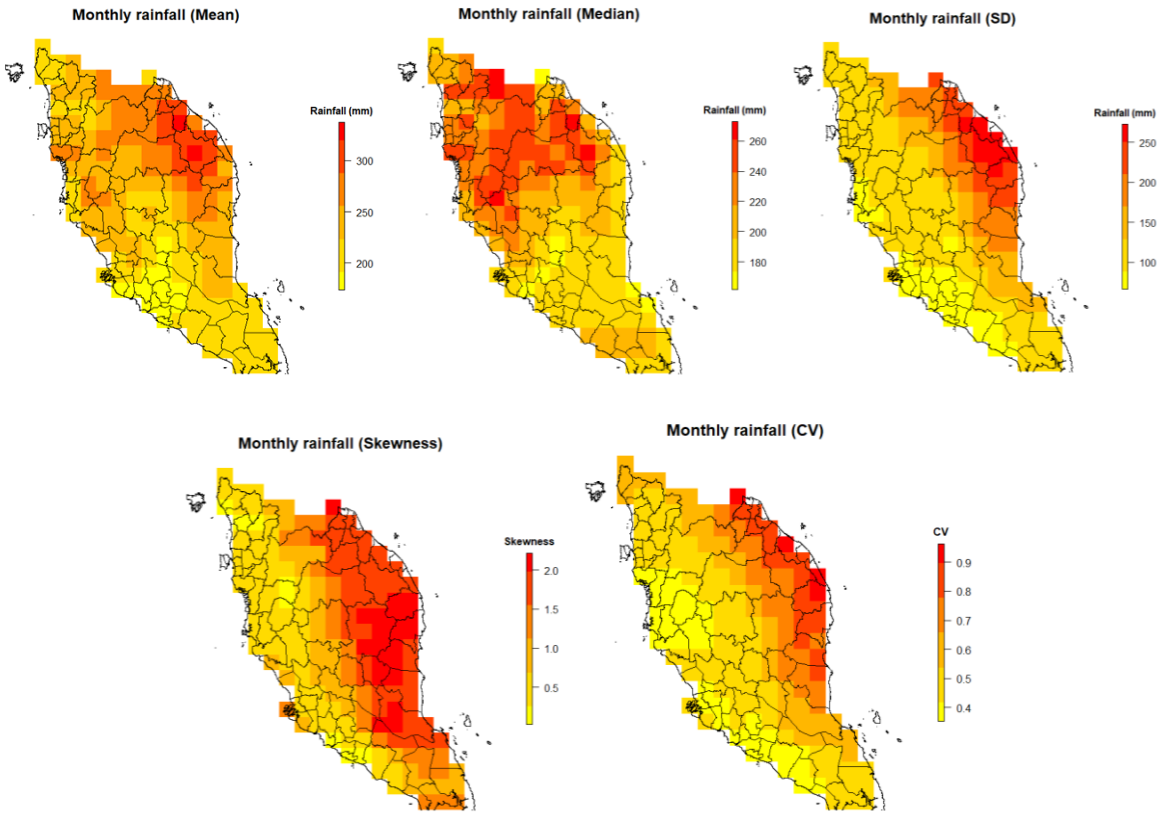

Figure 3. Spatial distribution of mean, median, SD, skewness, and CV of mean monthly rainfall in PM.

5.2 ENSO Influence Rainfall Spatial Pattern

The spatial distribution of cumulative rainfall during each ENSO event is presented in Figure 4. Similar to the findings by Muhammad et al. (2020) and Wong et al. (2016), it was visually observed that the spatial pattern of the cumulative rainfall during each ENSO event showed a high degree of variability across PM. For example, during the extreme El Niño events of 2015/2016, higher rainfall was observed along the western and northwestern coast, and a lower rainfall gradient was observed towards the southern region. On the other hand, during the strong La Niña events of 2010/2011, a similar high localized rainfall was observed in the central-southern region and the northeastern area. A gradient of lower rainfall was observed towards the northwestern and southwestern coasts. The spatial pattern of rainfall can be characterized by spatial dispersion, randomness, or clustering. The Moran's I statistic was computed for rainfall during different ENSO events (Soibam et al., 2015). Moran's I values are positive in each case, suggesting a spatial autocorrelation in rainfall distribution for each event. For extreme El Niño 2015/2016, it is 0.0946;

for strong La Niña 2010/2011, it is 0.2273. The positive values indicate that nearby locations tend to have similar values for each variable. The expected Moran's I values under the assumption of spatial randomness are consistently close to zero, and the standard deviations are relatively small. Additionally, the p-values associated with the observed Moran's I for all variables are 0, indicating that the spatial autocorrelation is statistically significant. Similar to the findings by Soibam et al. (2015), these results collectively suggest a notable spatial structure in the rainfall distribution during each ENSO event, emphasizing the importance of considering spatial relationships when analyzing these environmental variables.

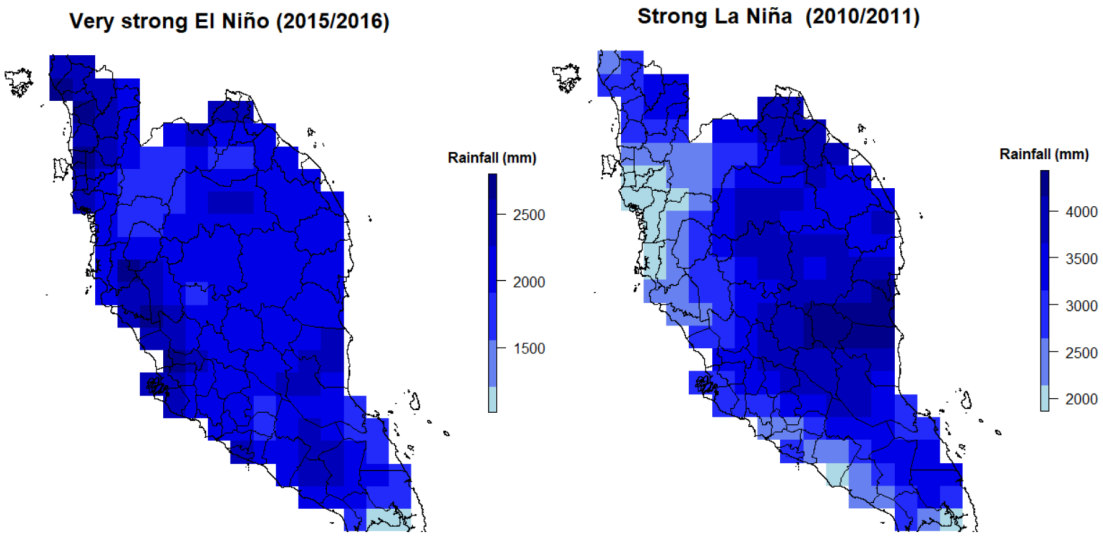

Figure 4. Spatial distribution of cumulative rainfall during the selected ENSO events.

5.3 Ordinary Least Squared Regression

The ANOVA test compared the RSS from an OLS regression with those from a GWR. This test is based on the methodology described by Brunsdon et al. (2002). The output provides several key statistics. The F-statistic is 2.6623, which measures the ratio of the variance explained by the model to the unexplained variance. The degrees of freedom (df) are provided for both the GWR model (df1 = 167.000) and the residuals (df2 = 89.299). These values are calculated based on the number of data points and effective parameters used in the GWR model, with an adjustment for the comparison. The p-value is 4.156e-07, indicating the probability of observing an F-statistic as extreme as 2.6623 under the null hypothesis that the GWR model does not significantly improve the fit compared to the OLS model. The very small p-value suggests that the GWR model

substantially improves the fit. The alternative hypothesis is that the GWR model explains more variance than the OLS model, which is supported by the small p-value. The sample estimates provide the sum of squares of the residuals for both the OLS model (SS OLS residuals = 197.39475) and the GWR model (SS GWR residuals = 74.14394). These values measure the total variance that each model fails to explain. The results of the ANOVA test indicate that the GWR model significantly reduces the RSS compared to the OLS model. The F-statistic of 2.6623, combined with the extremely small p-value, provides strong evidence against the null hypothesis, suggesting that the GWR model captures spatial variability in the data more effectively than the OLS model. The substantial reduction in the RSS further supports this conclusion, demonstrating that the GWR model provides a better fit by accounting for local variations in the relationship between the variables.

5.4 Weighting Function Comparison

Several performance metrics were assessed to compare the effectiveness of different weighting functions in GWR. These metrics include the AIC, AICc, quasi-global R^2, RSS, traceS, and sigma (model: traceS). The findings are summarized in Table 1. The evaluation of weighting functions across different ENSO events reveals distinct preferences for model performance. Both weighting functions exhibit suboptimal performance for the El Niño 2015/2016 event. Still, the Gaussian function holds a slight edge with an AIC of 398.48 compared to 434.12 for the Bisquare, although both display low Quasi-global R^2 values (0.63 for Gaussian and 0.48 for Bisquare), indicating inadequate model fit. In the La Niña 2010/2011 event, the performance of both weighting functions declined, with the Bisquare function marginally outperforming the Gaussian, achieving an AIC of 442.01 compared to 505.69. However, both exhibit low Quasi-global R^2 values (0.10 for Gaussian and 0.52 for Bisquare), highlighting insufficient model performance.

The choice of weighting function significantly influences model performance, particularly during different phases of the ENSO, such as El Niño and La Niña events. The Gaussian weighting function proved more effective during the El Niño 2015/2016 event, likely due to its bell-shaped curve, which assigns higher weights to nearby observations while diminishing the influence of more distant data points. This characteristic allows the Gaussian function to capture the more homogeneous climatic conditions often associated with El Niño, where broad-scale influences create a more precise signal in the data. The smoothing effect of the Gaussian function helps

stabilize estimates and manage extreme weather outliers, contributing to a lower AIC of 398.48 compared to 434.12 for the Bisquare function, alongside a marginally higher Quasi-global R^2 value of 0.63 versus 0.48. Conversely, the Bisquare weighting function demonstrated superior performance during the La Niña 2010/2011 event, as indicated by its lower AIC of 442.01 compared to the Gaussian's 505.69. This effectiveness can be attributed to the Bisquare function's robustness against outliers; it assigns lower weights to observations that deviate significantly from the fitted model. During La Niña, the increased variability and potential outliers, particularly in regions experiencing extreme rainfall, can affect model estimates, making the Bisquare function more suitable for capturing localized effects. Despite both weighting functions exhibiting low Quasi-global R^2 values, the Bisquare's value of 0.52 outperforms the Gaussian's 0.10, suggesting that it better models the specific responses associated with La Niña conditions. Overall, the Gaussian weighting function proves more effective for the El Niño 2015/2016, while the Bisquare weighting function slightly outperforms the La Niña 2010/2011 event. Therefore, Gaussian was used for El Niño 2015/2016, and Bisquare was used for La Niña 2010/2011 in the subsequent analysis.

Table 1. Comparison of weighting function under different studied ENSO events.

ENSO	Weighting Function	AIC	AICc	Quasi-global R^2	RSS	Sigma (model: traceS)
El Niño 2015/2016	Gaussian	398.48	523.88	0.63	74.14	0.820
	Bisquare	434.12	493.45	0.48	104.39	0.890
La Niña 2010/2011	Gaussian	505.69	515.14	0.10	189.63	1.080
	Bisquare	442.01	535.00	0.52	101.48	0.920

5.5 Spatial Patterns of The NDVI – Rainfall Relationship

Figure 5 represents local R^2 values obtained from GWR models for different ENSO events. It measures the proportion of the variance in the dependent variable explained by the GWR model at each location. The local R^2 values obtained from GWR models for different ENSO events provide information into the spatial variability of the relationship between NDVI and rainfall. The spatial pattern of local R^2 values (Figure 5(a)) shows notable differences between the El Niño (2015/2016) and La Niña (2010/2011) events. For the El Niño event, local R^2 values are generally higher, with

many areas indicating values closer to 0.6 to 0.8. This suggests that GWR models explain a significant portion of the spatial variability in these regions during a strong El Niño. The relatively uniform distribution of reduced rainfall and its effects on vegetation, as measured by the NDVI, allowed the GWR model to leverage local relationships effectively. During El Niño, the climatic conditions tend to be more consistent across larger areas, facilitating stronger correlations between NDVI and rainfall.

In contrast, the La Niña event map shows more widespread areas with slightly lower local R^2 values. Some areas also show a lower explanatory power, with local R^2 values dropping below 0.4 in some regions. The extreme rainfall associated with La Niña leads to more localized and variable effects on vegetation, making it more challenging for the GWR model to identify consistent relationships across different regions. As such, the variability in rainfall and its impact on NDVI during La Niña conditions may be more fragmented, resulting in less effective model performance. The boxplot (Figure 5(b)) summarises local R^2 values for both ENSO events. The median local R^2 for the El Niño event appears higher than that for La Niña, suggesting that the GWR model explained more spatial variability during El Niño conditions. The interquartile range for both events is similar, but the El Niño boxplot shows a slightly higher spread towards the upper end. Both distributions have a few outliers with negative R^2 values, indicating regions where the model fit was poor.

The lower R^2 values observed for the GWR model, particularly during La Niña events, stem from its sensitivity to local variations. While GWR captures spatial heterogeneity, it can introduce noise, especially in regions with highly variable NDVI-rainfall relationships, as seen during La Niña, where extreme rainfall variability causes fragmented impacts on vegetation, making it challenging to establish consistent relationships. Additionally, GWR may face issues such as multicollinearity, spatial autocorrelation, and insufficient data in certain regions, further reducing its explanatory power. Lessani and Li (2024) introduce the Similarity and Geographically Weighted Regression (SGWR) model to address these limitations. This enhances GWR by integrating a weight matrix that combines data attribute similarity with geographic proximity, improving performance across various statistical measures. Similarly, Liu et al. (2024) propose an improved semi-parametric Geographically Weighted Regression (ISGWR) approach, which modifies the spatial weight matrix to explain heterogeneity and non-stationarity in spatial relationships better, further enhancing model performance. Although beyond the scope of the current work, these

improved versions of GWR offer promising potential to address its limitations and enhance model performance.

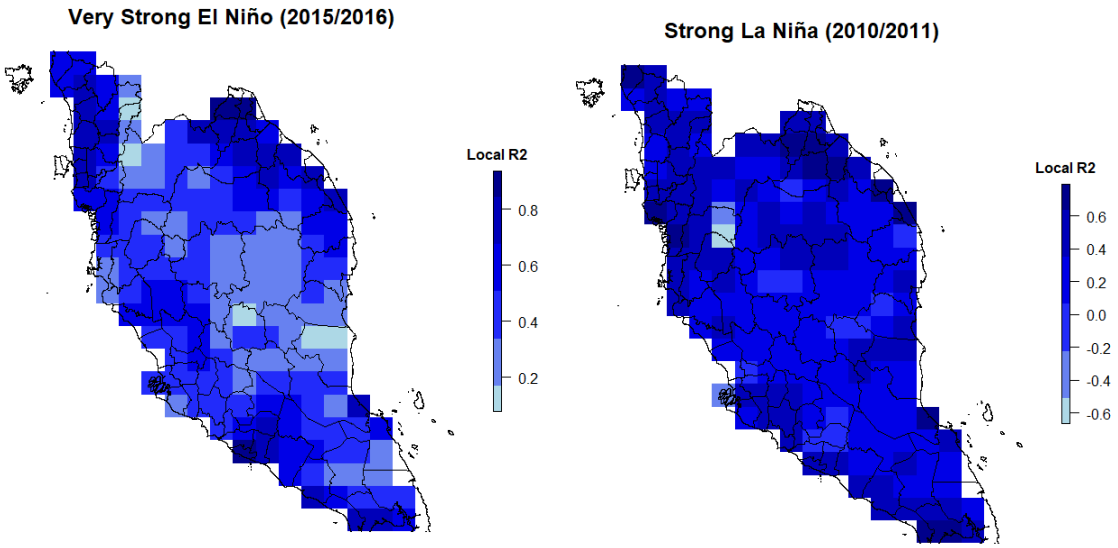

(a)

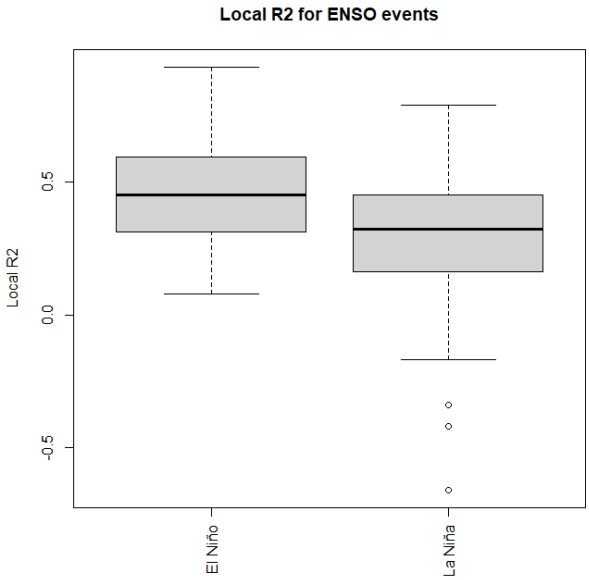

(b)

Figure 5. (a) Spatial distribution of local R^2 patterns, and (b) boxplot of local R^2 for the respective ENSO events. Low values suggest inadequate model performance and may indicate the potential absence of variables in the model.

Additionally, incorporating variables like soil type, land use, or elevation could reduce unobserved spatial heterogeneity while testing alternative spatial weighting functions in GWR could enhance local pattern capture. Pre-processing techniques such as spatial smoothing or temporal aggregation may also reduce variability from extreme weather events and improve model performance. Nonetheless, the overall findings affirm that GWR captured the spatial variation of climate impacts more effectively during the El Niño event than during La Niña in PM, likely due to the more uniform and predictable climatic conditions associated with El Niño compared to the variability and extremes introduced by La Niña.

The observed spatial variability of rainfall coefficients across PM during the El Niño 2015/2016 and La Niña 2010/2011 showed a negative value at 64% and 50% grid points, respectively (Figure 6). During El Niño events 2015/2016, a negative relationship was observed in the PM's northern, central-west and western regions. This indicates a non-linear relationship between rainfall and NDVI spatially across PM. The findings suggest that, with stronger El Niño events, an increase in rainfall is associated with a decrease in NDVI, implying a negative relationship in these regions. This is because the drier-than-average conditions in these regions typically result in reduced relative rainfall that is insufficient to cater to the need for vegetation growth (Tan et al., 2021; Tangang et al., 2017). High maximum temperatures, especially with reduced rainfall during El Niño events, can contribute to drought stress (Tan et al., 2021). Even with increased rainfall, if high temperatures persist, the water may evaporate quickly, reduce soil moisture, and enhance evapotranspiration, leaving less water available for vegetation. Previous work by Luo et al. (2018) also reported a highly uncertain photosynthesis reduction from rainforests during El Niño events 2015/2016 event. Besides, plants have different temperature thresholds beyond which their physiological processes are negatively affected (Khor et al., 2021).

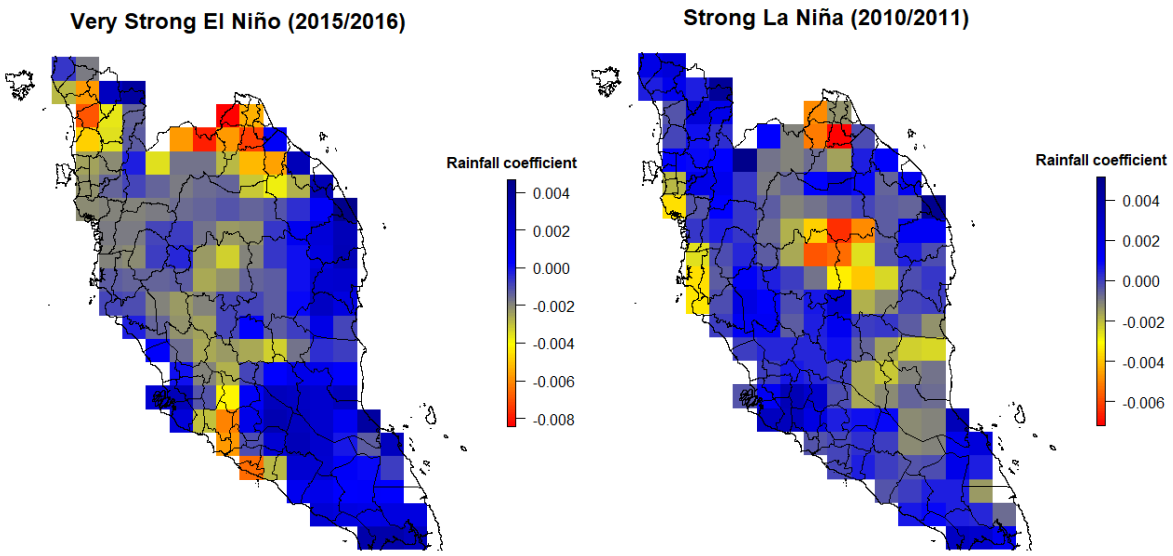

Figure 6. Rainfall coefficients during the selected ENSO events. The coefficients related to rainfall illustrate the extent of change in NDVI for a spatial unit with a corresponding increase in a spatial unit of rainfall.

These findings highlight the vulnerability of vegetation to the combined effects of reduced relative rainfall and high maximum temperatures, which exacerbate drought stress by reducing soil moisture and increasing evapotranspiration. This relationship highlights the importance of adaptive agricultural policies, including promoting drought-resistant crop varieties and adjusting planting schedules to mitigate the impacts of El Niño. For instance, Evamoni et al. (2023) identified drought-tolerant rice genotypes (MR185, MR211, MR253, MR269, MR284, MR303, and MR307) exhibiting superior biochemical responses, such as increased levels of total soluble sugar, proline, catalase, and ascorbate peroxidase, thereby advancing the application of these markers to improve drought tolerance and mitigate water scarcity in rice production. Similarly, Shamsudin et al. (2016) developed drought-tolerant lines of the Malaysian rice cultivar MR219 by pyramiding three drought-yield QTLs, achieving yield gains of 903–2523 kg ha−1 under drought stress, which contributes to sustainable agriculture and enhances food security in the face of water scarcity and climate change. Additionally, the results can inform ecosystem management strategies, including prioritizing reforestation or conservation efforts in drought-prone areas and enhancing water resource management to support vegetation growth under extreme climatic conditions. Therefore, reforestation in Malaysia, guided by government initiatives to restore degraded lands and to improve forest cover for biodiversity conservation and climate regulation, should prioritize

drought-prone areas to maximize ecological and climate resilience while actively involving local communities to ensure sustainability and foster shared responsibility for forest preservation (Saharudin et al., 2024). By integrating these findings into policy frameworks, stakeholders can better address the challenges posed by ENSO-induced variability in agriculture and ecosystems in the region.

Nonetheless. a positive relationship was observed in the eastern and southern regions during the El Niño events. This might be because the southern region has low-lying soil types, such as peat soil, with better water retention capabilities; therefore, increased rainfall during El Niño events could improve soil moisture levels, supporting positive vegetation growth. While El Niño events are generally associated with warmer temperatures, the southern region might experience temperatures conducive to plant growth without reaching stress levels. Meanwhile, in the eastern region of PM, a positive relationship between these variables can be attributed to the proximity to the South China Sea influences local climatic conditions, leading to localized weather changes during El Niño that enhance rainfall. This additional moisture is vital for vegetation, improving soil conditions and nutrient availability, promoting plant growth and elevating NDVI values. Furthermore, the eastern region's diverse ecosystems are well-adapted to seasonal variations, allowing them to capitalize on the increased rainfall effectively. When this rainfall coincides with critical growth periods for vegetation, the impact on NDVI becomes even more pronounced.

On the other hand, a positive association was observed during the La Niña events compared to the El Niño (Figure 4). However, the study identified significant variations in the rate of positive change, highlighting a localized decrease in the north-western coast, northeast, central region, and southeast coast. Certain localized areas may experience negative responses to La Niña conditions. Interestingly, the northeastern region showed a negative response, even though these regions consistently receive high rainfall, particularly during the NEM. This indicates that there may be a point of saturation where additional rainfall has diminishing returns in terms of promoting vegetation growth, as previously reported by Li et al. (2019). Once the soil is saturated, excess water may also lead to runoff and flooding rather than being absorbed by vegetation, limiting the positive impact on NDVI. Most of the vegetation in this area may reach a threshold beyond which additional water does not contribute substantially to their growth. Besides, the irregular or sporadic extreme rainfall might not support sustained vegetation growth as effectively as evenly distributed

rainfall in this area (Silveira et al., 2013). The sandy soils along the northeastern coast may drain water more quickly, influencing how effectively it utilizes increased rainfall for vegetation growth.

These findings highlight the necessity of adaptive agricultural and ecosystem management policies, such as optimizing water management, promoting soil conservation, and selecting vegetation suited to local soil and hydrological conditions to enhance resilience to irregular and extreme rainfall. The Muda Irrigation Scheme, managed by MADA, exemplifies sustainable water management by ensuring water availability for paddy cultivation while addressing food security through effective governance and environmental protection, offering a replication model in similarly affected PM areas (Man et al., 2023). Nasir Ahmad et al. (2024) emphasize that addressing the challenges of extreme rainfall in agriculture requires a comprehensive approach. Soil conservation practices, such as contour farming, terracing, and cover cropping, are vital for minimizing erosion and enhancing water retention, especially in high-elevation rainfall areas in the central region. Effective drainage systems, including ditches, drains, and retention basins, help manage excess water, mitigating flooding and protecting crops. Rainwater harvesting reduces erosion during heavy rains while providing an additional water source during dry periods. Crop rotation and diversification improve soil stability and sustain productivity by utilizing varied root structures and nutrient requirements. Mulching shields soil surfaces from raindrop impact, retains moisture and stabilizes soil conditions during variable rainfall. Other than that, educating farmers on sustainable practices will fosters better soil management, crop selection, and erosion control, enhancing resilience to extreme rainfall conditions.

During the El Niño events, high rainfall variability can lead to localized ecological responses, impacting vegetation dynamics differently across the landscape. A positive correlation between NDVI and rainfall may prevail in areas with consistent and abundant rain, indicating that increased rainfall fosters vegetation growth. Conversely, in regions where rainfall is less reliable or experiences significant fluctuations, the NDVI-rainfall relationship may be more complex, with vegetation responding differently to other factors. This observed variability underscores the importance of considering local factors and heterogeneity when examining the NDVI-rainfall relationship. Even though a positive rainfall coefficient was observed during La Niña events, the magnitude of change can also be different. The findings showed that a region-specific understanding of ecosystem dynamics is required to understand the NDVI-rainfall relationship, as

high rainfall variability across PM contributes to the diverse ecological responses observed in the study.

5.6 Performance of The Predicted Pattern

The spatial distribution of iNDVI, derived from GWR for the selected ENSO events (El Niño 2015/2016 and La Niña 2010/2011), shows distinct patterns across the study region (Figure 7). During the extreme El Niño event, the iNDVI values predominantly range from 6 to 10. The map reveals that most areas are between 8 and 10, with some regions showing slightly lower iNDVI values closer to 6, suggesting a moderate level of vegetation stress likely due to the warmer and drier conditions typically associated with El Niño. In contrast, the spatial distribution during the strong La Niña event shows generally higher iNDVI values, with a range predominantly between 8 and 11. In the central and northern regions, iNDVI values reach 11. This suggests that vegetation health and productivity were comparatively higher during La Niña, consistent with the cooler and wetter conditions usually linked to La Niña phases. The spatial contrast between these two ENSO events highlights the impact of climatic variations on vegetation, with iNDVI values indicating stronger vegetation response and potentially improved productivity during La Niña compared to El Niño.

The statistical evaluation of observed NDVI against iNDVI for the studied ENSO events highlights significant differences in model performance across several key metrics (Table 2). The MAE was 0.5 for the El Niño event, compared to 0.58 for La Niña, indicating that the predicted NDVI values during El Niño were closer to the observed values on average. Additionally, the RMSE was lower during El Niño at 0.66, while it was 0.77 for La Niña, suggesting that the model's predictions were more precise during the El Niño period, reflecting less deviation from the observed values. Furthermore, the R^2 was 0.63 for El Niño and 0.52 for La Niña, indicating that the model explained a more significant proportion of the variance in observed NDVI during El Niño conditions. The NSE metric, which assesses the predictive power of hydrological models, showed a value of 0.63 for El Niño and 0.52 for La Niña, reinforcing that the model's predictions were more effective during the El Niño event. Lastly, the KGE was calculated at 0.6 for El Niño and 0.5 for La Niña, confirming the model's superior performance in capturing the relationship between observed NDVI and iNDVI under El Niño conditions. These metrics suggest that the model better captured the relationship between observed NDVI and iNDVI during the El Niño

event than the La Niña event, underscoring its enhanced accuracy and reliability under varying climatic conditions.

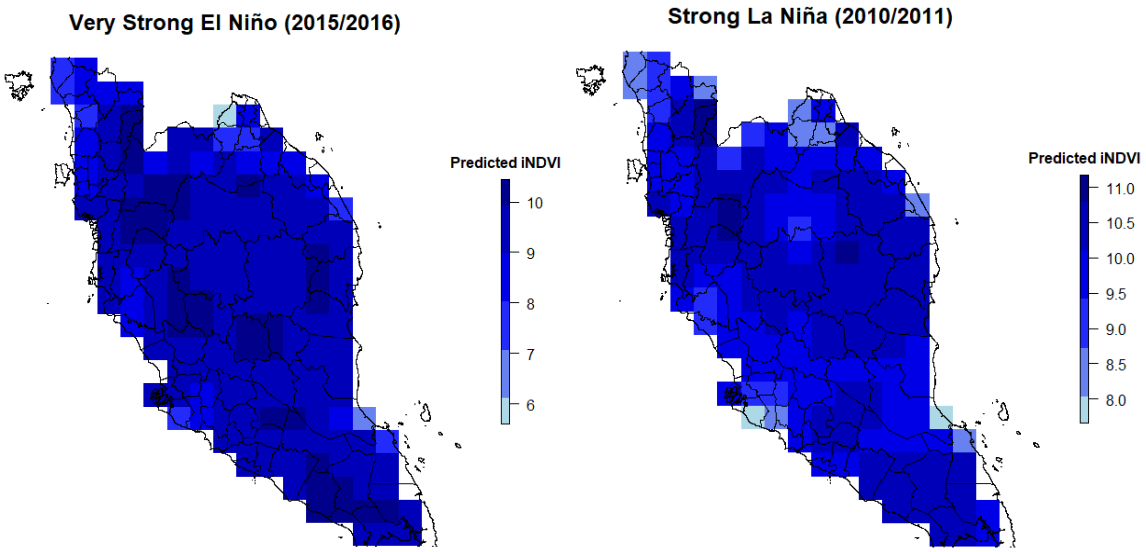

Figure 7. Spatial distribution of iNDVI during the selected ENSO events.

Table 2. Statistical evaluation of the observed NDVI against iNDVI.

Metric	El Niño (2015/2016)	La Niña (2010/2011)
MAE	0.5	0.58
RMSE	0.66	0.77
R^2	0.63	0.52
NSE	0.63	0.52
KGE	0.6	0.5

6.0 Conclusion

GWR is a dynamically adaptive tool for detecting geographical relationships, leveraging local information to achieve a more refined distribution. This results in predicting a smoother pattern of NDVI response, explaining a higher variance and effectively mitigating autocorrelation in the residuals. However, when faced with extreme climate variability, such as an ENSO event, the intricate mechanism influencing the relationship between NDVI and rainfall must consider additional factors with a strong local impact, such as soil type, human disturbances (urbanization),

vegetation thresholds during extremely wet and warm periods, and unique local climatic conditions. These localized variations highlight that the spatial patterns of NDVI exhibit different magnitudes of positive or negative correlations with rainfall in various PM parts. The study suggests that while rainfall predominantly determines vegetation growth, other factors may lead to negative influences. Specifically, the southern parts of the PM generally display stronger correlations, likely attributed to the abundance of water, low-lying areas, and diverse plant species that can adapt to contrasting warmer conditions during El Niño and wetter conditions during La Niña. These findings showed that the GWR model can be used for a larger regional scale across PM under the influence of El Niño. Still, a more specific localized region should be identified to simulate a homogeneous (increasing or decreasing) relationship under the influence of La Niña.

In tropical regions like PM, GWR allows regression parameters to vary spatially, revealing diverse temporal and spatial patterns in the direction and strength of the NDVI-rainfall correlation. The study highlights this relationship's spatial heterogeneity and non-stationarity by mapping local diagnostics. These findings emphasize the importance of integrating adaptive agricultural strategies, sustainable water management practices, and targeted ecosystem conservation efforts to enhance resilience against drought and extreme rainfall, safeguarding food security and promoting ecological sustainability amid climate variability. The findings indicate that GWR is a practical alternative to OLS modelling in areas with heterogeneity sensitive to environmental and climate variations. The GWR approach provides superior predictions, reduces autocorrelation in the residuals, and highlights local variations. These initial findings, focused on optimizing the GWR model, will serve as a foundation for subsequent analyses incorporating additional variables to offer a more comprehensive view of the factors influencing vegetation behaviour. Physical variables (e.g., soil type, land use, elevation) and climate variables (e.g., wind speed, temperature, solar radiation, humidity) are currently being integrated to address the complexities introduced by high variability scenarios in PM. Future work will extend this analysis by incorporating these variables into the GWR model, enhancing understanding of their influence on NDVI responses and providing a more holistic view of the complex interactions shaping vegetation dynamics in tropical regions like PM. Furthermore, the different NDVI and rainfall datasets can be compared to evaluate the robustness and consistency of the findings.

Acknowledgement

This work was supported by UTM Professional Development Research University Special (Grant No. R.J130000.7113.07E66).

References

Arjasakusuma, S., Yamaguchi, Y., Hirano, Y., & Zhou, X. (2018). ENSO and rainfall-sensitive vegetation regions in Indonesia as identified from multi-sensor remote sensing data. *ISPRS International Journal of Geo-Information*, *7*(3), 103. https://doi.org/10.3390/ijgi7030103

Balaghi, R., Tychon, B., Eerens, H., & Jlibene, M. (2008). Empirical regression models using NDVI, rainfall and temperature data for the early prediction of wheat grain yields in Morocco. *International Journal of Applied Earth Observation and Geoinformation*, *10*(4), 438-452. https://doi.org/10.1016/j.jag.2006.12.001

Bechtold, U. (2018). Plant life in extreme environments: how do you improve drought tolerance? *Frontiers in plant science*, *9*, 543. https://doi.org/10.3389/fpls.2018.00543

Bhatti, U. A., Tang, H., Khan, A., Ghadi, Y. Y., Bhatti, M. A., & Khan, K. A. (2024). Investigating the nexus between energy, socio-economic factors and environmental pollution: A geo-spatial multi regression approach. *Gondwana Research*, *130*, 308-325. https://doi.org/10.1016/j.gr.2024.02.007

Born, J., Bagchi, R., Burslem, D., Nilus, R., Tellenbach, C., Pluess, A. R., & Ghazoul, J. (2015). Differential responses of dipterocarp seedlings to soil moisture and microtopography. *Biotropica*, *47*(1), 49-58. https://doi.org/10.1111/btp.12180

Boyd, D. S., Phipps, P. C., Foody, G. M., & Walsh, R. P. D. (2002). Exploring the utility of NOAA AVHRR middle infrared reflectance to monitor the impacts of ENSO-induced drought stress on Sabah rainforests. *International Journal of Remote Sensing*, *23*(23), 5141-5147. https://doi.org/10.1080/01431160210163128

Brunsdon, C., Fotheringham, A. S., & Charlton, M. (2002). Geographically weighted summary statistics—a framework for localised exploratory data analysis. *Computers, Environment and Urban Systems*, *26*(6), 501-524. https://doi.org/10.1016/S0198-9715(01)00009-6

Chew, Y. J., Ooi, S. Y., Pang, Y. H., & Wong, K. S. (2022). A Review of forest fire combating efforts, challenges and future directions in Peninsular Malaysia, Sabah, and Sarawak. *Forests*, *13*(9), 1405. https://doi.org/10.3390/f13091405

Evamoni, F. Z., Nulit, R., Ibrahim, M. H., Sidek, N., Kong Yap, C., & Yong Seok Yien, C. (2023). Evaluation of the drought tolerance level of Malaysian indica rice genotypes using biochemical markers at reproductive stage. *Chilean journal of agricultural research*, *83*(6), 742-753. https://doi.org/10.4067/S0718-58392023000600742

Pereira Filho, A. J., Vemado, F., Vemado, G., Gomes Vieira Reis, F. A., Giordano, L. D. C., Cerri, R. I., ... & Amaral, C. D. S. (2018). A step towards integrating CMORPH precipitation estimation with rain gauge measurements. *Advances in Meteorology*, *2018*(1), 2095304. https://doi.org/10.1155/2018/2095304

Gaviria, J., Turner, B. L., & Engelbrecht, B. M. (2017). Drivers of tree species distribution across a tropical rainfall gradient. *Ecosphere*, *8*(2), e01712. https://doi.org/10.1002/ecs2.1712

Geniaux, G. (2024). Speeding up estimation of spatially varying coefficients models. *Journal of Geographical Systems*, *26*(3), 293-327. https://doi.org/10.1007/s10109-024-00442-3

Georganos, S., Abdi, A. M., Tenenbaum, D. E., & Kalogirou, S. (2017). Examining the NDVI-rainfall relationship in the semi-arid Sahel using geographically weighted regression. *Journal of Arid Environments*, *146*, 64-74. https://doi.org/10.1016/j.jaridenv.2017.06.004

Gumindoga, W., Rientjes, T. H. M., Haile, A. T., Makurira, H., & Reggiani, P. (2019a). Performance evaluation of CMORPH satellite precipitation product in the Zambezi Basin. *International journal of remote sensing*, *40*(20), 7730-7749. https://doi.org/10.1080/01431161.2019.1602791

Gumindoga, W., Rientjes, T. H., Haile, A. T., Makurira, H., & Reggiani, P. (2019b). Performance of bias-correction schemes for CMORPH rainfall estimates in the Zambezi River basin. *Hydrology and Earth System Sciences*, *23*(7), 2915-2938. https://doi.org/10.5194/hess-23-2915-2019

Houmsi, M. R., Ismail, Z. B., Ziarh, G. F., Hamed, M. M., Ishak, D. S. B. M., Muhammad, M. K. I., ... & Shahid, S. (2023). Relative Influence of Meteorological Variables of Human Thermal Stress in Peninsular Malaysia. *Sustainability*, *15*(17), 12842. https://doi.org/10.3390/su151712842

Huang, S., Tang, L., Hupy, J. P., Wang, Y., & Shao, G. (2021). A commentary review on the use of normalized difference vegetation index (NDVI) in the era of popular remote sensing. *Journal of Forestry Research*, *32*(1), 1-6. https://doi.org/10.1007/s11676-020-01155-1

Joyce, R. J., Janowiak, J. E., Arkin, P. A., & Xie, P. (2004). CMORPH: A method that produces global precipitation estimates from passive microwave and infrared data at high spatial and temporal resolution. *Journal of Hydrometeorology*, *5*(3), 487-503. https://doi.org/10.1175/1525-7541(2004)005%3C0487:CAMTPG%3E2.0.CO;2

Kang, L., Di, L., Deng, M., Shao, Y., Yu, G., & Shrestha, R. (2014). Use of geographically weighted regression model for exploring spatial patterns and local factors behind NDVI-precipitation correlation. *IEEE Journal of Selected Topics in Applied Earth Observations and Remote Sensing*, *7*(11), 4530-4538. https://doi.org/10.1109/JSTARS.2014.2361128

Khor, J. F., Ling, L., Yusop, Z., Tan, W. L., Ling, J. L., & Soo, E. Z. X. (2021). Impact of El Niño on oil palm yield in Malaysia. *Agronomy*, *11*(11), 2189. https://doi.org/10.3390/agronomy11112189

Lamchin, M., Park, T., Lee, J. Y., & Lee, W. K. (2015). Monitoring of vegetation dynamics in the Mongolia using MODIS NDVIs and their relationship to rainfall by natural zone. *Journal of the Indian Society of Remote Sensing*, *43*, 325-337. https://doi.org/10.1007/s12524-014-0366-8

Lessani, M. N., & Li, Z. (2024). SGWR: similarity and geographically weighted regression. *International Journal of Geographical Information Science*, 1-24. https://doi.org/10.1080/13658816.2024.2342319

Li, L., Zheng, Z., Biederman, J. A., Xu, C., Xu, Z., Che, R., ... & Hao, Y. (2019). Ecological responses to heavy rainfall depend on seasonal timing and multi-year recurrence. *New Phytologist*, *223*(2), 647-660. https://doi.org/10.1111/nph.15832

Lion, M., Kosugi, Y., Takanashi, S., Noguchi, S., Itoh, M., Katsuyama, M., ... & Shamsuddin, S. A. (2017). Evapotranspiration and water source of a tropical rainforest in peninsular Malaysia. *Hydrological Processes*, *31*(24), 4338-4353. https://doi.org/10.1002/hyp.11360

Liu, Z., Li, Y., Gruyer, D., Zargayouna, M., & Tu, M. (2024). Exploring the spatial relationship between urban built environment and green travel: An improved semi-parametric GWR approach. *International Journal of Transportation Science and Technology*. https://doi.org/10.1016/j.ijtst.2024.07.008

Luo, X., Keenan, T. F., Fisher, J. B., Jiménez-Munoz, J. C., Chen, J. M., Jiang, C., ... & Tadić, J. M. (2018). The impact of the 2015/2016 El Niño on global photosynthesis using satellite

remote sensing. *Philosophical Transactions of the Royal Society B: Biological Sciences*, *373*(1760), 20170409. https://doi.org/10.1098/rstb.2017.0409

Mallick, J., AlMesfer, M. K., Singh, V. P., Falqi, I. I., Singh, C. K., Alsubih, M., & Kahla, N. B. (2021). Evaluating the NDVI–rainfall relationship in Bisha watershed, Saudi Arabia using non-stationary modeling technique. *Atmosphere*, *12*(5), 593. https://doi.org/10.3390/atmos12050593

Marryanna, L., Noguchi, S., Kosugi, Y., Niiyama, K., Itoh, M., Sato, T., ... & Abd-Rahman, K. (2019). Spatial Distribution of Soil Moisture and Its Influence on Stand Structure in a Lowland Dipterocarp Forest in Peninsular Malaysia. *Journal of Tropical Forest Science*, *31*(2), 135-150. https://doi.org/10.26525/jtfs2019.31.2.135150

Mohd Razali, S., Marin Atucha, A. A., Nuruddin, A. A., Abdul Hamid, H., & Mohd Shafri, H. Z. (2016). Monitoring vegetation drought using MODIS remote sensing indices for natural forest and plantation areas. *Journal of Spatial Science*, *61*(1), 157-172. https://doi.org/10.1080/14498596.2015.1084247

Mondiana, Y. Q., Pramoedyo, H., Iriany, A., & Marjono, M. (2024, September). Fixed effect geographically weighted panel regression: A comparison of Kernel Gaussian and Bi-Square for modeling sugarcane yield in East Java. In *AIP Conference Proceedings* (Vol. 3235, No. 1). AIP Publishing. https://doi.org/10.1063/5.0234584

Moses, O., Blamey, R. C., & Reason, C. J. (2022). Relationships between NDVI, river discharge and climate in the Okavango River Basin region. *International Journal of Climatology*, *42*(2), 691-713. https://doi.org/10.1002/joc.7267

Muhammad, M. K. I., Shahid, S., Hamed, M. M., Harun, S., Ismail, T., & Wang, X. (2022). Development of a temperature-based model using machine learning algorithms for the projection of Evapotranspiration of Peninsular Malaysia. *Water*, *14*(18), 2858. https://doi.org/10.3390/w14182858

Muhammad, N. S., Abdullah, J., & Julien, P. Y. (2020, May). Characteristics of rainfall in peninsular Malaysia. In *Journal of Physics: Conference Series* (Vol. 1529, No. 5, p. 052014). IOP Publishing. https://doi.org/10.1088/1742-6596/1529/5/052014

Nasir Ahmad, N. S. B., Mustafa, F. B., & Muhammad Yusoff, S. Y. (2024). Spatial prediction of soil erosion risk using knowledge-driven method in Malaysia's Steepland Agriculture

Forested Valley. *Environment, Development and Sustainability*, *26*(6), 15333-15359. https://doi.org/10.1007/s10668-023-03251-8

Man, N. K. N., Ismail, N. E., Zakaria, N. A., & Chang, C. K. (2023). Agriculture irrigation development in Kedah, Malaysia: Strengthen the linkage between national food and water security. In *Water Projects and Technologies in Asia* (pp. 303-313). CRC Press. https://doi.org/10.1201/9781003222736-30

O'Sullivan, D. (2003). Geographically weighted regression: the analysis of spatially varying relationships. *Geographical Analysis*, *35*(3), 272-275. https://doi.org/10.1353/geo.2003.0008

Pang, G., Wang, X., & Yang, M. (2017). Using the NDVI to identify variations in, and responses of, vegetation to climate change on the Tibetan Plateau from 1982 to 2012. *Quaternary International*, *444*, 87-96. https://doi.org/10.1016/j.quaint.2016.08.038

Saharudin, D. M., Jeswani, H. K., & Azapagic, A. (2024). Reforestation of tropical rainforests as a negative emissions technology in Malaysia: An environmental and economic sustainability assessment. *Journal of Environmental Management*, *371*, 123250. https://doi.org/10.1016/j.jenvman.2024.123250

Shamsudin, N. A. A., Swamy, B. M., Ratnam, W., Sta. Cruz, M. T., Raman, A., & Kumar, A. (2016). Marker assisted pyramiding of drought yield QTLs into a popular Malaysian rice cultivar, MR219. *BMC Genetics*, *17*, 1-14. https://doi.org/10.1186/s12863-016-0334-0

Silveira, A. P., Martins, F. R., & Araújo, F. S. (2013). Do vegetative and reproductive phenophases of deciduous tropical species respond similarly to rainfall pulses? *Journal of Forestry Research*, *24*(4), 643-651. https://doi.org/10.1007/s11676-013-0366-5

Soibam, I., Nilima, N., & Phanjoubam, S. (2015). "Investigation of Rainfall-NDVI Spatial Variation - Geographical Weighted Regression Approach." *International Journal of Computing, Communication and Instrumentation Engineering* 2 (2). Science and Education Publishing Co., Ltd.: 24–27. doi:10.12691/AJMSE-2-2-3.

Tan, M. L., Juneng, L., Tangang, F. T., Chung, J. X., & Radin Firdaus, R. B. (2021). Changes in temperature extremes and their relationship with ENSO in Malaysia from 1985 to 2018. *International Journal of Climatology*, *41*(S1), E2564-E2580. https://doi.org/10.1002/joc.6864

Tangang, F., Farzanmanesh, R., Mirzaei, A., Supari, Salimun, E., Jamaluddin, A. F., & Juneng, L. (2017). Characteristics of precipitation extremes in Malaysia associated with El Niño and La

Niña events. *International Journal of Climatology*, *37*, 696-716. https://doi.org/10.1002/joc.5032

Udelhoven, T., Stellmes, M., del Barrio, G., & Hill, J. (2009). Assessment of rainfall and NDVI anomalies in Spain (1989–1999) using distributed lag models. *International Journal of Remote Sensing*, *30*(8), 1961-1976. https://doi.org/10.1080/01431160802546829

Wang, K. H., & Hamzah, M. Z. (2018). Different cambial activities in response to climatic factors of three Malaysian rainforest Shorea species with different stem diameters. *Trees*, *32*, 1519-1530. https://doi.org/10.1007/s00468-018-1730-z

Xu, S., Wu, C., Wang, L., Gonsamo, A., Shen, Y., & Niu, Z. (2015). A new satellite-based monthly precipitation downscaling algorithm with non-stationary relationship between precipitation and land surface characteristics. *Remote Sensing of Environment*, *162*, 119-140. https://doi.org/10.1016/j.rse.2015.02.024

Yamada, H. (2024). Geary'sc for Multivariate Spatial Data. *Mathematics*, *12*(12), 1820. https://doi.org/10.3390/math12121820

Zhang, X., Wu, S., Yan, X., & Chen, Z. (2017). A global classification of vegetation based on NDVI, rainfall and temperature. *International Journal of Climatology*, *37*(5), 2318-2324. https://doi.org/10.1002/joc.4847

Zhao, Z., Gao, J., Wang, Y., Liu, J., & Li, S. (2015). Exploring spatially variable relationships between NDVI and climatic factors in a transition zone using geographically weighted regression. *Theoretical and Applied Climatology*, *120*, 507-519. https://doi.org/10.1007/s00704-014-1188-x